J. Fluid Mech. (2013), *vol.* 725, *pp.* 588–610. © Cambridge University Press 2013
doi:10.1017/jfm.2013.112

Dense gravity currents moving beneath progressive free-surface water waves

T. O. Robinson[1],†, I. Eames[2] and R. Simons[1]

[1]Department of Civil, Environmental and Geomatic Engineering, University College London, Gower Street, London WC1E 6BT, UK

[2]Department of Mechanical Engineering, University College London, Torrington Place, London WC1E 7JE, UK

(Received 10 May 2012; revised 31 October 2012; accepted 20 February 2013; first published online 23 May 2013)

The characteristics of dense gravity currents in coastal regions, where free-surface gravity waves are dominant, have yet to be studied in the laboratory. This paper provides a first insight into the dynamics of dense saline gravity currents moving beneath regular progressive free-surface water waves. The gravity currents were generated by releasing a finite volume of saline into a large wave tank with an established periodic wave field. After the initial collapse, the gravity currents propagated horizontally with two fronts, one propagating in the wave direction and the other against the wave direction. The fronts of the gravity currents oscillated with an amplitude and phase that correlated with the orbital velocities within a region close to the bed. To leading order, the overall length of the gravity current was found to be weakly affected by the wave action and the dynamics of the current could be approximated by simply considering the buoyancy of the released fluid. Other characteristics such as the position of the gravity current centre and the shape of the two leading profiles were found to be significantly affected by the wave action. The centre was displaced at constant speed dependent on the second-order wave-induced mean Lagrangian velocity. For long waves, the centre was advected downstream in the direction of wave propagation owing to the dominance of Stokes drift. For short waves, the gravity current centre moved upstream against the wave direction, as under these wave conditions Stokes drift is negligible at the bed. An asymmetry in the shape of the upstream and downstream current heads was observed, with the gravity current front moving against the waves being much thicker and the front steeper, similar to the case of a current moving in a stream.

Key words: gravity currents, multiphase flow, surface gravity waves

1. Introduction

Gravity currents encompass a wide range of density-driven (compositional, temperature or salinity variation) horizontal flows, which have been generated by a vertical hydrostatic imbalance in the density of two adjacent fluids. For these types of flows a density interface is formed between the gravity current and the ambient flow. The current dynamics are described in terms of the position of the leading edge of the density interface and the characteristics of the gravity current head. The available

† Email address for correspondence: tristan.robinson@ucl.ac.uk

https://doi.org/10.1017/jfm.2013.112 Published online by Cambridge University Press

literature on gravity currents is fairly broad and dates from the pioneering work by von Kármán (1940). The natural occurrences and the environmental impacts of gravity currents (Simpson 1997) are known and the theoretical concepts available to describe such phenomena are at an advanced stage (Huppert 2006).

In the coastal environment, applications of this work relate to dense plumes at estuaries (e.g. salt wedges), oceanographic boundaries (e.g. Atlantic meridional overturning circulation), anthropogenic interventions (e.g. dredging spoils) and industrial out-fall (e.g. desalination plants). These examples illustrate that gravity currents have the potential to transport material over a considerable distance. However, other transport and mixing processes caused by tides, currents and wave action are more commonly associated with transport of material in this environment. Nielsen (1992) provides a good overview of these processes for regions near the seabed.

The coupled effect of density-driven flows with additional forcing from the ambient flow has the potential to modify how material or chemical components from these gravity currents are transported in coastal waters. The propagation of the gravity currents in horizontal ambient flows has been investigated by Simpson & Britter (1979), Bühler, Wright & Kim (1991) and Kranenburg (1993). The Lagrangian dispersion of gravity currents propagating with two fronts in uniform ambient flows has been studied both experimentally and theoretically by Hallworth, Hogg & Huppert (1998), Hogg, Huppert & Hallworth (2005) and Slim & Huppert (2008). In these studies, it was observed that the ambient velocity generated asymmetries in the position and shape of the two density interface fronts. Although there is some on-going work to resolve the internal dynamics and the difference in the observed profiles, the essential physics of the Lagrangian propagation (frontal velocities and positions) of the gravity currents appear to be well captured by the constant-Froude-number and source conditions (Hallworth *et al.* 1998). The two effects of buoyancy-driven motion and the mean flow are essentially additive and the ambient flow advects dense saline currents at approximately 60 % of the ambient flow speed.

The coupled effect of buoyancy-driven motion and forcing by waves has only been considered in a few studies (Chamberlain 2000; Ng & Fu 2002), although its importance has been observed in the field by Wright *et al.* (1988) and Wright, Friedrichs & Scully (2001) and been coupled to numerical models for oil spill risk management (Skogness & Johansen 2004). Wright *et al.* (1988, 2001) studied salt wedges, described as gravity-driven underflows, at the Yellow River delta in China and showed that, under certain conditions, waves played an important role in controlling the transport of suspended silt. However, there were no measurements of the wave-induced flows nor a description of the gravity current characteristics for different wave conditions.

Ng & Fu (2002) analysed theoretically the effect of progressive free-surface water waves on the dispersion of finite volumes of dense viscous gravity currents. They demonstrated that in shallow water, transport by streaming dominated over the buoyancy, and this dominance was reversed for deep water. However, in all cases it was observed that the presence of the waves enhanced the flow in the wave direction and acted as a counterflow in the opposite direction at a rate proportional to the near-bottom Lagrangian mean velocity. It should be noted that Ng & Fu (2002) used an eddy viscosity (taken as 10^2–10^4 larger than the kinematic viscosity of water) which formed the basis of the omission of inertia from their analysis and the assumption that the gravity currents were thinner than the boundary layer. In contrast our study focuses on the case when the boundary layer is turbulent and gravity currents are inertially dominant.

https://doi.org/10.1017/jfm.2013.112 Published online by Cambridge University Press

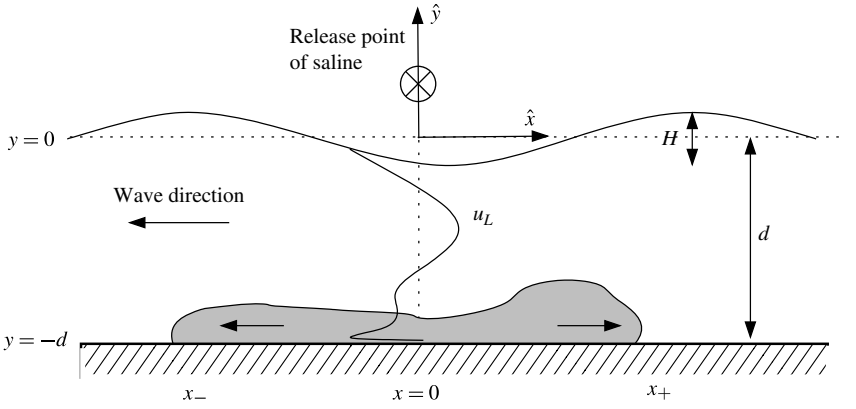


FIGURE 1. Schematic of the problem considered. Saline fluid is introduced at ⊗ into a wave field with a Lagrangian mass flux profile u_L and wave height H. The fronts of the gravity current propagate distance x_- and x_+, downstream and upstream respectively.

In the present paper, we examine how the spreading of inertia-dominant gravity currents is affected by progressive free-surface waves. The aim is to better understand the dispersion of gravity currents in the coastal environment. The work is primarily an experimental study that employs a configuration which is idealized compared to many in the natural environment. The regular wave field, which is used to force the gravity currents, enables the results to be characterized in a quantitative manner. To provide a framework to interpret the experimental results, we present a box model of the gravity current dynamics. This includes forcing by the orbital wave motion and second-order wave-induced flows. The novel part of the experimental component is the high temporal resolution of the observations that makes it possible to quantify the rapid movement of the gravity current head caused by the orbital motion, and the application of different flow visualization techniques to quantify the effect of the wave motion on the shape of the gravity current head.

This paper is structured as follows: in § 2, the experimental setup and diagnostics that are applied are described. The generated wave characteristics are described in § 3. A theoretical model of the gravity current dynamics in the presence of waves is presented in § 4. The results from the experimental study are presented in § 5 in terms of gravity current lengths, displacement of the gravity current centres and shape of the current heads. These results are discussed in relation to previous studies and the conclusions are given in § 6.

2. Experimental setup and diagnostics

The experiments were carried out in a glass-sided wave tank 12 m long, 45 cm wide and filled with water to a depth $d = 40$ cm. The wave tank had active absorption piston-type wave-makers installed at both ends of the channel, which enabled low-frequency shallow water waves with periods in the range ($0.8\ \text{s} < T < 2.5\ \text{s}$) to be generated at one end of the tank and absorbed at the other end. At the centre of the flume the gravity current was generated by releasing a finite volume of saline from a reservoir placed above the flume. A schematic of the system under investigation is shown in figure 1.

https://doi.org/10.1017/jfm.2013.112 Published online by Cambridge University Press

2.1. *Wave generator*

Progressive free-surface waves were generated by the oscillation of a wave board using a force-controlled wave-maker and using a corrective wave actuator signal to reduce the second-order effects at the wave board. An absorbing paddle is designed to remove any reflected waves. The system is closed and hence a wave-induced circulation is set up by any wave-induced mean flow. The free-surface wave profiles were measured using four resistance probes; three were attached to a mobile platform and one remained static. This setup allowed the wave profiles to be measured at a number of points along the flume.

The horizontal and vertical components of the wave-induced velocity field were measured along a vertical axis beneath the waves using a laser-Doppler velocimeter (LDV) (Innova 70C 5-Watt argon-ion laser and a two-component TSI laser anemometer), which was mounted on a 3-axis motorized traverse. The LDV was placed at mid-length along the side of the flume and a motorized traverse was used to place the focal point of the laser beams along a vertical water column, which corresponds horizontally to the centre point, $x = 0$, of the flume and vertically at the bed, $y = -d$ (see figure 1).

2.2. *Gravity current generation*

The gravity currents were generated by releasing finite volumes V_r of saline, density ρ_r, from a reservoir placed above the ambient water (density ρ_a, where $\rho_r > \rho_a$) surface. The reservoir consisted of a funnel, located above the free surface in the centre of the flume at $x = 0$ (as shown in figure 1), with a 3.4 cm diameter outlet and adjustable height to accommodate for variable wave heights. An alternative reservoir, which released saline across the width of the flume, was found to create a greater splash as it entered the water. The chosen system allowed the saline to penetrate the wave field with minimal impact on the wave form.

A similar release method was used by Hallworth *et al.* (1998) and Hogg & Huppert (2001) to study the dispersion of gravity currents in uniform ambient flows. As the dense fluid descended, it entrained ambient fluid, reducing the density of the horizontal propagating gravity current. An initial mixing factor of 20 ± 2 was measured (Robinson 2007), which is similar to the values reported by Hallworth *et al.* (1998) and Hogg & Huppert (2001). In the study of gravity currents, it is common to express the density difference in terms of the reduced gravity. Hence, in this case, the initial reduced gravity, g'_r, of the discharged fluid is

$$g'_r = g\left(\frac{\rho_r - \rho_a}{\rho_a}\right), \tag{2.1}$$

where g is the gravitational acceleration, given as $g = 981$ cm s^{-2}.

The initial buoyancy of released fluid is $g'_r V_r$ and two-dimensional horizontal propagation (as shown in figure 1) is characterized in terms of $g'_r A_r$, where A_r is the volume of the released fluid divided by the channel width. The buoyancy term is not affected by the dilution as $g'_r A_r = g' A$ where g' and A are respectively the reduced gravity and cross-sectional area of the horizontal gravity current. The experimental results in § 5 are presented in terms of initial reduced gravity g'_r, that varied from 20 to 50 cm s^{-2}, and initial released volume V_r, that varied from 600 to 1800 cm^3. The Reynolds number range of the generated gravity currents is limited as the initial reduced gravity (g'_r) is substantially diluted (by a factor of 20) during the release phase of the saline. For the case of static ambient water, Huppert & Simpson (1980)

https://doi.org/10.1017/jfm.2013.112 Published online by Cambridge University Press

have shown that the gravity current may experience four propagation regimes (release, quasi-steady, inertia and viscous). The present work describes inertia-dominant weakly turbulent laminar gravity currents. For these types of density flows it has been shown that the influence of the Schmidt number is negligible (Dahm & Dimotakis 1990; Mueschke *et al.* 2009) and does not need to be taken into account. The viscous gravity current propagating in wave fields has been studied by Ng & Fu (2002).

Other techniques for releasing a gravity current were tested, including the more standard lock release (Rottman & Simpson 1983; Shin, Dalziel & Linden 2004; Adduce, Sciortino & Proietti 2012). However, the standard lock release technique required placing vertical gates within the wave tank. This was found to interfere with the mean flow generated by the oscillatory boundary layers which takes time to become fully established (Longuet-Higgins 1953; Swan 1990). This method was deemed not appropriate for these types of experiments. Alternative injection methods were found to distort the free-surface profile and introduce additional components to the wave motion. The chosen method was found to give consistent and reproducible results.

2.3. *Gravity current diagnostics*

To follow and record the continuous progression of the gravity currents, a traverse, which ran along one side of the length of the flume, was built. On the opposite side of the tank, light boxes with diffusers were installed to provide a uniform light backdrop. The sidewalls of the tank were glass panels (100 cm $\times$ 80 cm) but vertical supporting structural columns obscured the view over parts of the tank. Potassium permanganate was added to the released fluid to distinguish the gravity current fluid from the ambient water. The vertical descent and subsequent horizontal propagation of the dense current was measured with the aid of a monochrome camera (Pulnix TM-9701 machine vision camera), which was mounted on the traverse carriage to film the progression of the gravity current fronts. The relative position of the camera along the tank was determined using markers placed on the tank and bespoke image processing algorithms (Matrox Imaging Library). The camera was connected to a frame grabber card (Matrox Meteor-II/Standard analogue frame grabber card) and image recognition software (Matrox Inspector V1.0) was used to capture the images. The width-averaged images of the saline propagation were analysed using a combination of bespoke and standard image processing tools (Matrox Inspector V1.0 and Matlab V6.5 with the Image Processing Toolbox) to determine the front positions, dimensions of the current head and the density concentrations of the released fluid. Density concentrations of the gravity current head were measured by calculating the attenuation of background light related to the potassium permanganate in the gravity current. The methodology of using the light intensity to infer the dye concentration of a fluid has been extensively applied in the past, for instances by Hacker, Linden & Dalziel (1996), Hogg & Huppert (2001) and Marino, Thomas & Linden (2005).

In addition to the width-averaged gravity current profiles a limited number of tests were carried out using the laser-induced fluorescence (LIF) technique to capture thin vertical slices of the gravity current head. These tests were carried out at a fixed upstream and downstream position. Unlike the width-averaged method the LIF system was not designed to track the gravity current as it propagated in the flume. A pulse laser (dual YAG laser), set at a 7.5 Hz, was used to generate the laser light sheet and a monochrome camera (Pulnix TM-9701) to capture the images. In these tests, sodium fluorescein was added to the gravity current fluid, which in contact with the laser sheet acts as a fluorescent tracer. The laser light sheet, parallel to the flume, was projected

https://doi.org/10.1017/jfm.2013.112 Published online by Cambridge University Press

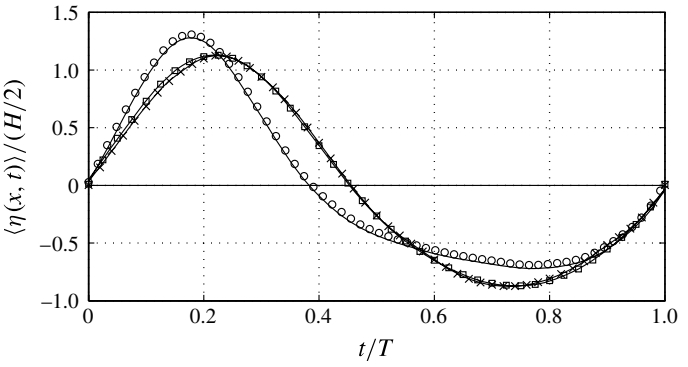


FIGURE 2. The dimensionless ensemble wave height profiles $\langle\eta(x,t)\rangle/(H/2)$ are plotted as a function of dimensionless time t/T. The measured free surfaces ($\times$, $\square$ and $\bigcirc$) are compared to (3.1) (solid lines) for waves with periods T and wave heights ($H = 0.80$ s, 6.49 cm; 1.60 s, 6.05 cm; and 2.46 s, 7.00 cm respectively) for cases W2, W4 and W6 in table 1.

through the free surface along the centre of the flume at $x_\pm = \pm 145$ cm. This laser configuration produced an area with a maximum view of 60 cm at the bed. As the gravity current passes through the laser light sheet a thin ($0.01 \sim 0.02$ cm) clear image of the gravity current is produced. For the short waves with large amplitudes this setup was found to be problematic because the curvature of the free surface caused light to scatter, which resulted in irregular lighting in the water column. Considering this limitation of the LIF setup, the images were used to visualize the instabilities along the density interface that cannot be seen from the width-averaged images. For these LIF tests no light intensity measurements were derived as a proxy for the density concentration.

3. Characterization of the wave field

3.1. *Free-surface profile*

Ensemble averages of the free-surface profiles are shown as a function of time under different wave conditions in figure 2. A summary of the wave characteristics is given in table 1. The wave free-surface profile, $\eta(x,t)$, was characterized by

$$\eta(x,t) = \sum_{n=1}^{N} \left[a_n \sin(k_n x + \omega_n t) + b_n \cos(k_n x + \omega_n t)\right], \tag{3.1}$$

where $\omega_n = 2n\pi/T$ is the angular frequency and the wavenumber k_n is determined from the dispersion relationship (3.8). Under the assumption that the wave propagates with a slow change in form, the parameters a_n and b_n are determined from the weighted integrals of $\langle\eta\rangle \sin k_n x$ and $\langle\eta\rangle \cos k_n x$, where $\langle\rangle$ denotes an ensemble average at a fixed position in the flume. The wave height, H, is determined from the ensemble profiles and corresponds to the vertical distance between the wave crest and wave trough. The sharp crests and shallow troughs, as shown in figure 2, are characteristics of second-order waves and are implicit in Stokes second-order wave theory (Milne-Thomson 1968). In practice, further complications arise due to the effects of sidewalls, free second-order harmonic waves and reflections.

https://doi.org/10.1017/jfm.2013.112 Published online by Cambridge University Press

https://doi.org/10.1017/jfm.2013.112 Published online by Cambridge University Press

Test no.	T (s)	H (cm)	a_1 (cm)	b_1 (cm)	$\overline{u}_{min}$ (cm s^{-1})	$\overline{u}_{max}$ (cm s^{-1})	$\overline{v}_{min}$ (cm s^{-1})	$\overline{v}_{max}$ (cm s^{-1})	$\overline{u}_E$ (cm s^{-1})	$\overline{u}_S$ (cm s^{-1})	$\overline{u}_L$ (cm s^{-1})
W1	0.80	3.35	1.69	0.13	−1.67	2.01	−0.35	0.36	0.24	−0.05	0.19
W2	0.80	6.49	3.15	0.44	−2.94	3.96	−0.65	0.52	0.91	−0.19	0.72
W3	1.60	2.95	1.48	0.11	−5.63	5.49	−0.33	0.34	−0.14	−0.14	−0.31
W4	1.60	6.05	2.97	0.44	−11.34	10.39	−0.64	0.71	−0.16	−0.70	−0.86
W5	2.46	3.30	1.59	0.34	−8.03	6.62	−0.38	0.31	−0.39	−0.27	−0.67
W6	2.46	7.00	2.98	1.04	−16.73	12.31	−0.77	0.53	−0.47	−0.98	−1.45

TABLE 1. Summary of wave properties and wave-induced flows. The mean velocities (3.10) are depth averaged over the 5 cm measured from the bottom of the flume. See the text for definitions.

3.2. *Wave-induced flow*

Surface waves generate an orbital motion in the water column. The oscillatory motion adjacent to the free surface (on which a shear-free condition is applied) and adjacent to the rigid floor (on which a non-slip condition is applied) set up boundary layers and a streaming flow. Vorticity is advected from both ends, the bottom of the flume and the free surface. Since the water is bounded by vertical walls, mass conservation requires that the average volume flux along any vertical plane is zero. The velocity field $\boldsymbol{u}(\boldsymbol{x}, t)$ can be decomposed as

$$\boldsymbol{u}(\boldsymbol{x}, t) = \boldsymbol{u}_O(\boldsymbol{x}, t) + u_E\hat{\boldsymbol{x}}, \tag{3.2}$$

where $\boldsymbol{u}_O$ is the oscillatory (orbital) flow and

$$u_E(y) = \frac{1}{T_m}\int_0^{T_m} \boldsymbol{u}\cdot\hat{\boldsymbol{x}}\,\mathrm{d}t, \tag{3.3}$$

is the mean velocity where T_m is the averaging time. Taking the average over one period T is not enough because the measurements are Eulerian and any experimental errors (velocities and wave periods) may lead to inacurracies in calculations of the mean flow results. To ensure accurate measurements of the wave-induced mean flow the averaging time is taken as $T_m \gg T$. Measurements were taken along a vertical y-axis at the centre of the flume ($x = 0$).

The orbital motion is largely dominated by the potential flow generated by the progressive waves. Using (3.1) and a linearized analysis (Lighthill 1978) of the flow generated by progressive waves, the horizontal and vertical components of oscillatory flow in (3.2) are given as

$$u_O(\boldsymbol{x}, t) = \sum_{n=1}^{N}\left[\frac{-\omega_n\cosh(y+d)k_n}{\sinh dk_n}\left(a_n\sin(k_nx+\omega_nt) + b_n\cos(k_nx+\omega_nt)\right)\right], \tag{3.4a}$$

$$v_O(\boldsymbol{x}, t) = \sum_{n=1}^{N}\left[\frac{\omega_n\sinh(y+d)k_n}{\sinh dk_n}\left(a_n\cos(k_nx+\omega_nt) - b_n\sin(k_nx+\omega_nt)\right)\right]. \tag{3.4b}$$

Figure 3 shows a hodograph plot of the Eulerian measurements of the velocity field at fixed points and the orbital velocities predicted by (3.4). As the wave-induced flows are given by (3.2), the mean Eulerian components were subtracted from the measured velocities in figure 3. The agreement with measured orbital velocities is quite good except at large wave amplitudes, where the effect of higher-order components changes the wave form (Stokes 1847). Contrary to the visual impression of figure 3, the mean orbital velocities measured over a wave period were zero. This is due to the temporal asymmetry in the orbital motion shown in figure 2.

Irrotational oscillatory motion sets up a steady streaming motion, often referred to as Stokes drift, see Longuet-Higgins (1953), Johns (1970) and Swan & Sleath (1990). Eulerian measurements (at fixed points) fail to pick up this contribution to the mass flux profile. It was attempted to measure the Lagrangian mass flux profile by following dye lines created by dropping and sinking crystals of potassium permanganate (Bagnold 1946; Dyke & Barstow 1981) but the inaccuracy and inconsistency in this technique was considerable.

The streaming motion can only be quantified by analysing the motion of fluid elements advected by the Lagrangian velocity (3.2). A fluid particle at $\boldsymbol{x}_0$ moves

https://doi.org/10.1017/jfm.2013.112 Published online by Cambridge University Press

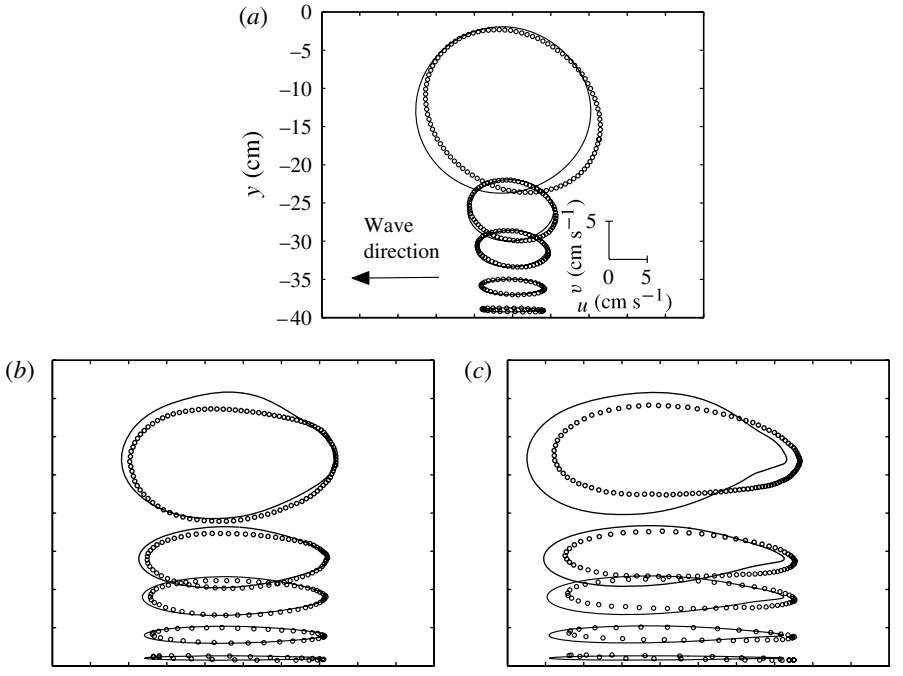


FIGURE 3. A hodograph of the measured horizontal and vertical orbital velocity trajectories (◯) compared with those from (3.4) for $N = 10$ (solid lines). Positions of the orbital velocities in the water column are $y = -13, -26, -31$ and -39 cm as indicated in the y-axis in (a) and the magnitude of the orbital velocities are given in the insert axis in (a). The wave period, T, and wave height, H, are (a) 0.80 s and 6.49 cm, (b) 1.60 s and 6.05 cm and (c) 2.46 s and 7.00 cm respectively for cases W2, W4 and W6 in table 1.

to $\boldsymbol{x}_0 + \boldsymbol{X}$ in time t, where

$$\frac{\mathrm{d}\boldsymbol{X}}{\mathrm{d}t} = \boldsymbol{u}(\boldsymbol{x}_0 + \boldsymbol{X}, t) = \boldsymbol{u}_O(\boldsymbol{x}_0 + \boldsymbol{X}, t) + u_E(y)\hat{\boldsymbol{x}}. \tag{3.5}$$

The mean Lagrangian, $u_L(y)$, horizontal motion of the fluid elements is defined as the average value of (3.5) over a long duration where $T_m \gg T$. This can be written as

$$u_L(y) = \frac{1}{T_m}\int_0^{T_m} \frac{\mathrm{d}\boldsymbol{X}}{\mathrm{d}t}\,\mathrm{d}t \cdot \hat{\boldsymbol{x}} = \frac{1}{T_m}\int_0^{T_m} \boldsymbol{u}_O(\boldsymbol{x}_0 + \boldsymbol{X}, t)\,\mathrm{d}t \cdot \hat{\boldsymbol{x}} + u_E(y). \tag{3.6}$$

From (3.5), we can show that to leading order $\boldsymbol{X} \sim \int \boldsymbol{u}_O\,\mathrm{d}t$, but substituting this into (3.6) leads to a convolution integral over time. When the flow is dominated by the irrotational component and is moving with constant phase speed, c_p, the convolution integral in (3.6) is reduced to give the Stokes drift term (Eames & McIntyre 1999)

$$u_S(y) = -\frac{1}{T_m c_p}\int_0^{T_m} |\boldsymbol{u}_O|^2\,\mathrm{d}t. \tag{3.7}$$

For this wave regime a first-order approximation of the wave celerity is given by

$$c_p^2 = \frac{g}{k_n}\tanh(k_n d). \tag{3.8}$$

https://doi.org/10.1017/jfm.2013.112 Published online by Cambridge University Press

The negative Stokes drift, in (3.7), is a consequence of the waves propagating in the direction of decreasing x (towards the left in figure 1). Substituting (3.4) into (3.7) gives

$$u_S(y) = -\sum_{n=1}^{\infty}(a_n^2 + b_n^2)k_n^2 c_p \frac{\cosh 2k_n(y+d)}{2\sinh^2 \mathrm{d}k_n}. \tag{3.9}$$

Similar expressions have been derived by others (Longuet-Higgins 1953; Johns 1970; Xu & Bowen 1994) although often only the first term in the summation is stated.

Figure 4 shows the variation, for $kd =$ (*a*) 2.5, (*b*) 0.9 and (*c*) 0.5, of the measured mean Eulerian velocity, u_E, Stokes drift, u_S (estimated from (3.7) and using the experimental velocity time series) and the Lagrangian mean velocity, u_L (determined from (3.6) where $u_L(y) = u_S(y) + u_E(y)$). The laboratory Lagrangian profiles are compared with Longuet-Higgins (1953) theory. For the long waves, figure 4(*b,c*), the theory correctly predicts the mass profile; however there are significant differences in the region near the bed. For the short waves, figure 4(*a*), the theoretical profile significantly overestimates the induced velocity. Similar observations were reported by Russell & Osorio (1957) and Swan (1990).

The results show that adjacent to the tank floor a thin streaming flow is generated in the wave direction and this is reversed within a few centimetres above the floor. For short waves, figure 4(*a*), the Stokes drift decays quickly with depth and the flow adjacent to the floor is dominated by the viscous boundary layer, which drives fluid in the opposite direction to the wave propagation. For longer waves, figure 4(*b,c*), both the orbital velocity and Stokes drift are weakly dependent on depth and dominate the viscous streaming flow, leading to a mean flow in the direction of wave propagation. As the wave period increases further, the magnitude of this streaming affect becomes more pronounced. The viscous boundary layer on the free surface and inviscid drift are both in the direction of waves. Since the total mass flux is zero, there is a return flow in the opposite direction to the wave movement.

The mean Lagrangian velocity shows a significant variation within a thin boundary layer adjacent to the tank floor beyond which the mean shear is weak. As we shall see later, the bulk movement of a dense gravity current is affected by the mean flow near the rigid floor. The mean flow in this region is averaged over a fixed depth as

$$\overline{u}_* = \frac{1}{d_a}\int_{-d}^{-d+d_a} \boldsymbol{u}_* \cdot \hat{\boldsymbol{x}}\, \mathrm{d}y, \tag{3.10}$$

where $* = E, S$ and L refer to previous velocity definitions and averaged is over a layer of thickness d_a adjacent to the rigid boundary. In the present study, the thickness of this layer is $d_a = 5$ cm, as this was observed to correspond to the typical vertical thickness of the gravity current. The average of the mean Lagrangian velocity, $\overline{u}_L$, demonstrates that while the oscillatory boundary layer adjacent to the rigid floor is large it has a negligible contribution to the total mass flux as it occurs in a thin layer.

The main difficulty in making an accurate comparison between measured mean Lagrangian velocity (incorporating Stokes drift and Eulerian velocity) and the theoretical predictions is imposing the correct boundary conditions at the wave forcing ends of the tank. Such profiles are sensitive to the nature of the forcing and can differ from one wave tank to another which tends to explain the lack of consensus in comparisons between theoretical models and measurements seen in the literature (Longuet-Higgins 1953; Russell & Osorio 1957; Swan 1990; Monismith *et al.* 2007).

https://doi.org/10.1017/jfm.2013.112 Published online by Cambridge University Press

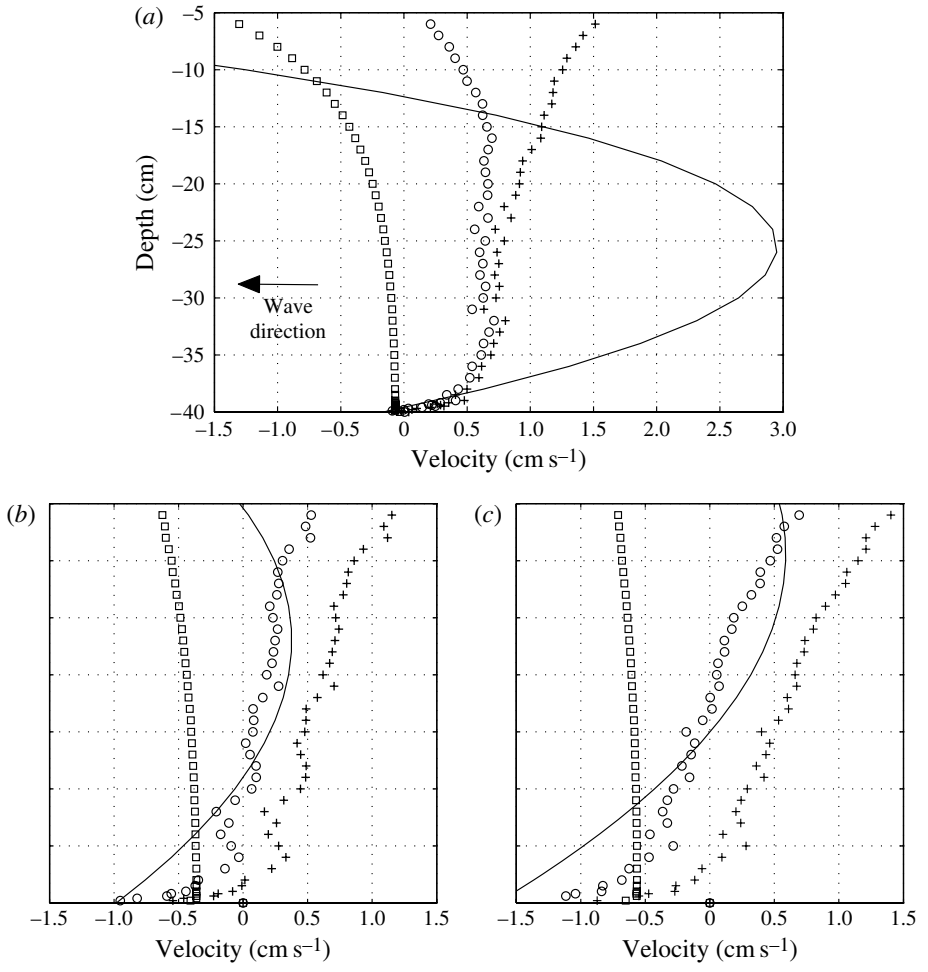


FIGURE 4. Vertical profiles of the mean wave-induced velocities beneath progressive free-surface water waves for (*a*) $T = 0.80$ s, $H = 6.49$ cm, (*b*) 1.60 s, 6.05 cm and (*c*) 2.46 s, 7.00 cm (cases W2, W4 and W6 in table 1). The symbols +, □ and ○ correspond to u_E, u_S and u_L respectively, and the solid line is the Longuet-Higgins (1953) theory.

4. Characterization of the gravity current in the presence of waves

The gravity current moves due to a combination of a buoyancy-driven component and the local instantaneous velocity field. To provide a means of interpreting the experimental measurements of a gravity current in the presence of waves we apply a methodology based on the standard box model (Huppert & Simpson 1980). This model has also been used to model gravity currents in the presence of uniform ambient flow (Hallworth *et al.* 1998). The basis of the box model is the assumption of conservation of volume, written as

$$\mathscr{L} = x_+ - x_- = \frac{A}{h}, \tag{4.1}$$

where h is the current height, assumed to be constant along the length of the gravity current. Although some asymmetry in the gravity current is expected (as illustrated in figure 1) at present we are unable to assess the magnitude of these variations and

https://doi.org/10.1017/jfm.2013.112 Published online by Cambridge University Press

hence, to first approximation, a constant height assumption is adopted. The theory presented does not take into account the spatial variations in the gravity current speed, height and density. In addition, the front velocity of the gravity current is defined by the Froude-number condition (Benjamin 1968; Huppert & Simpson 1980). The assumption of a constant Froude number has been used by Hallworth *et al.* (1998), Shin *et al.* (2004) and Hogg *et al.* (2005) to model accurately the propagation of gravity currents in a number of different systems and regimes. The present analysis will make use of this to derive first-order theoretical approximations.

In this study the gravity current is allowed to propagate in two directions within an orbital velocity field (3.2), see figure 1. Hence, the horizontal positions of the two leading current fronts with respect to time are given as

$$\frac{\mathrm{d}x_+}{\mathrm{d}t} = Fr\left(g'h\right)^{1/2} + u(x,t), \tag{4.2a}$$

$$\frac{\mathrm{d}x_-}{\mathrm{d}t} = -Fr\left(g'h\right)^{1/2} + u(x,t), \tag{4.2b}$$

where Fr is the Froude number used to characterize the speed of the fronts and the value is assigned from the experiments with no waves present. For the present test configuration the measured variation in Froude number is within the experimental error presented by Marino *et al.* (2005).

Apart from a very thin layer of the order of 0.1 cm thick, the wave-induced motion in the region close to the bed (thickness $d_a = 5$ cm) is predominantly horizontal ($u_{max} \gg v_{max}$) and the backwards and forwards oscillation is independent of depth, as shown in figure 3. In this region, the horizontal velocity field $u(x,t)$ is dominated by the first term in the expansion of (3.2)

$$u(x,t) \approx -\frac{\omega_1}{\sinh k_1 d}\left(a_1 \sin(k_1 x + \omega_1 t) + b_1 \cos(k_1 x + \omega_1 t)\right) + u_E. \tag{4.3}$$

As with the standard treatment and discussion of Stokes drift (Eames 2008), it is important to identify the rapidly and slowly varying forcing terms in (4.2). We express the gravity current positions $x_\pm$ in terms of rapidly $x_{\pm_R}$ and slowly $x_{\pm_S}$ varying contributions as $x_\pm = x_{\pm_R} + x_{\pm_S}$. As the wave period is much shorter than the advective time scale of the gravity current, the magnitude of the rapidly varying position of the current front due to the oscillatory wave-induced motion is approximated as

$$\frac{\mathrm{d}x_{\pm_R}}{\mathrm{d}t} \approx \frac{a_1\omega_1}{\sinh k_1 d}\sin(k_1 x_\pm + \omega_1 t). \tag{4.4}$$

Since $|a_1| \gg |b_1|$, the b_1 term is neglected (see table 1). Expanding (4.4) and using $k_1 x_{\pm_R} \ll 1$, which is consistent here since $k_1 a_1 = 2\pi a_1/\lambda \ll 1$ (see table 1), gives

$$\frac{\mathrm{d}x_{\pm_R}}{\mathrm{d}t} \approx -\frac{a_1 k_1 c_p}{\sinh k_1 d}\cos(k_1 x_{\pm_S} + \omega_1 t) - \frac{a_1^2 k_1^2 c_p}{\sinh^2 k_1 d}\sin^2(k_1 x_{\pm_S} + \omega_1 t). \tag{4.5}$$

Averaging (4.5) over one wave period provides the means of deriving a first-order approximation for the gravity current front positions propagating in the presence of a regular wave field

$$\frac{\mathrm{d}\langle x_+\rangle}{\mathrm{d}t} \approx Fr\left(g'h\right)^{1/2} - \frac{(a_1k_1)^2 c_p}{2\sinh^2 k_1 d} + u_E, \tag{4.6a}$$

$$\frac{\mathrm{d}\langle x_-\rangle}{\mathrm{d}t} \approx -Fr\left(g'h\right)^{1/2} - \frac{(a_1k_1)^2 c_p}{2\sinh^2 k_1 d} + u_E. \tag{4.6b}$$

https://doi.org/10.1017/jfm.2013.112 Published online by Cambridge University Press

These equations can be resolved by substituting (4.1) into (4.6) then adding and subtracting the resulting two equations to give

$$\langle x_+ \rangle = \frac{1}{2}(3Fr)^{2/3}\left(g'A\right)^{1/3}t^{2/3} + \left(u_E - \frac{(a_1k_1)^2c_p}{2\sinh^2 k_1 d}\right)t, \tag{4.7a}$$

$$\langle x_- \rangle = -\frac{1}{2}(3Fr)^{2/3}\left(g'A\right)^{1/3}t^{2/3} + \left(u_E - \frac{(a_1k_1)^2c_p}{2\sinh^2 k_1 d}\right)t, \tag{4.7b}$$

where it is taken that $x_+ = x_- = 0$ at $t = 0$. The expressions for the total length, $\mathscr{L}$, and position of the centre, $\mathscr{X} = (x_+ + x_-)/2$, of the gravity current are given as

$$\mathscr{L} = (3Fr)^{2/3}\left(g'A\right)^{1/3}t^{2/3}, \quad \mathscr{X} = \left(u_E - \frac{(a_1k_1)^2c_p}{2\sinh^2 k_1 d}\right)t. \tag{4.8a,b}$$

This derivation follows the methodology described by Hallworth *et al.* (1998) and could be extended to include all the wavenumber contributions to the oscillatory flow. The buoyancy term $g'A$ is equivalent to $g'_r A_r$, the excess mass of the released saline compared with fresh water.

The propagation, in terms of the total length, of gravity currents in stagnant fluid and in uniform ambient flow is well-known (Kranenburg 1993; Hallworth *et al.* 1998; Slim & Huppert 2008). In the present case the centre of the gravity current $\mathscr{X}$ is advected by a mean Lagrangian velocity, $\overline{u}_L$, which corresponds to a combination of the mean Eulerian velocity and Stokes drift ($\overline{u}_L = \overline{u}_E + \overline{u}_S$). The rate of displacement of the gravity current centre is given as

$$\frac{\mathrm{d}\mathscr{X}}{\mathrm{d}t} = \overline{u}_L. \tag{4.9}$$

The detailed studies by Hallworth *et al.* (1998) and Hogg & Huppert (2001) on saline and particle-driven gravity currents in a mean steady flow concluded that the current centre is advected at a fraction of the ambient flow (typically ~60 %).

5. Experimental measurements of the gravity current

The description of the experimental results is split into the movement of the fronts, the overall length of the current, displacement of the centroid position of the current and visualization of the shape of the current head.

5.1. *Front positions of the gravity current*

The two fronts of the gravity currents (downstream x_- and upstream x_+) were followed in time using low and high temporal resolution techniques. The high-resolution results required a bespoke image processing method to measure the relationship between the current movement and the wave frequency. This used images with sufficient temporal resolution that the rapid oscillation of wave action could be analysed, see figure 5. The method was capable of measuring the position of the gravity current front to within ±1 cm upstream and downstream from the point of release. The gaps in the data were caused where the flume supports obscured the head of the gravity current from the camera. The low temporal resolution method involved following the upstream and downstream gravity current fronts by eye and marking simultaneously the position of the leading edge of the fronts at 10 s intervals. This method was found to be accurate within a maximum error of ±7 cm, depending on the oscillation of the wave. Although the accuracy of the low temporal data was not sufficient to measure the

https://doi.org/10.1017/jfm.2013.112 Published online by Cambridge University Press

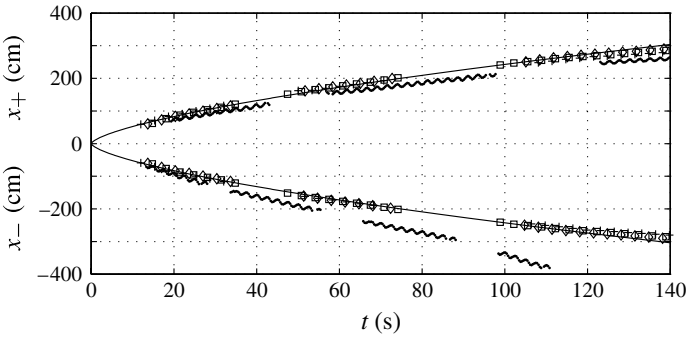


FIGURE 5. The position of the two fronts of the gravity current: $+, \square, \lozenge$ repeated experiments with no waves present and $\bullet$ (appears as oscillating solid line) with waves (case W6 in table 1), are shown as functions of time after release. In each case $V_r = 1200\ \text{cm}^3$ and $g_r' = 40$–$45\ \text{cm s}^{-2}$. The theoretical predictions from (4.7), with $Fr = 1.1$, of the gravity current fronts with the wave components turned off are shown with the solid lines.

intra-wave oscillation of the gravity current, it was accurate to give the position of the leading fronts as the maximum error reduces to 1.25 % of the gravity current length when fully dispersed. The oscillation of the current front was measured using a high-resolution digital video camera set at 30 frames per second with a measured local error of ± 0.2 cm. In practice, this method was found to be successful for front oscillations with amplitudes greater than 2 cm.

The experimental reproducibility is demonstrated in figure 5. This shows the results of repeated tests for a gravity current propagating in static ambient water. The results are in good agreement with the theoretical model (4.7), when the wave forcing components are turned off. The Froude number, determined from experiments, $Fr = 1.1 \pm 0.01$, was comparable to other studies. In the presence of long waves (case *W*6 in table 1), the gravity current dynamics were significantly altered by the wave forcing (figure 5). The downstream gravity current was found to propagate faster compared to the case of no wave forcing. In contrast, the upstream gravity current experienced a counterflow effect compared to the static ambient water case. This has an overall effect of shifting the gravity current centre in the wave direction.

The positions of the fronts were observed to oscillate at the same frequency as the wave. The amplitude (and phase) was tested by subtracting a local linear fit from the high temporal resolution of the front positions at each segment of the data (defined by the gaps in the data, see figure 5, due to the vertical supporting columns). The amplitude of the gravity current head oscillation at each section was found to remain constant. Hence, the orbital movement was observed to have an instantaneous effect on the gravity current dynamics. Using first-order theory (4.3), the magnitude of the horizontal displacement of the rapidly varying position of the gravity current front $\Delta x_\pm$ can be approximated as

$$\frac{\Delta x_\pm}{(a_1^2 + b_1^2)^{1/2}} = \frac{2}{\sinh k_1 d}. \tag{5.1}$$

Figure 6 shows a comparison between (5.1) and the experimental observations (see table 1 for wave conditions). The accuracy in the y-axis is ± 0.1; this comes from the error (± 0.2 cm) in measuring the amplitude of the gravity current front oscillation.

https://doi.org/10.1017/jfm.2013.112 Published online by Cambridge University Press

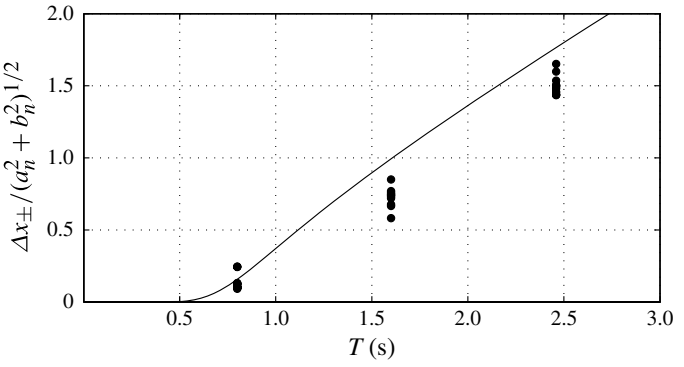


FIGURE 6. Non-dimensionalized mean amplitude of the gravity current oscillation (•) plotted against wave period for the wave conditions in table 1. The theoretical approximation (solid line) is given by (5.1).

Although there is some scatter in the data, the results are shown for multiple tests and demonstrate the underlying trends that are derived from the theoretical model.

5.2. *Total length of the gravity current*

The total length of the gravity current, $\mathscr{L}$, was measured by averaging the position of the moving current fronts over one wave period. The experimental observations shown in figure 7, using the low temporal resolution method to capture the front position, for three wave periods and four wave heights are compared with the theoretical model (4.7) in the absence of wave forcing and $Fr = 1.1$. These results illustrate the overall effect of the wave motion on the gravity current propagation. The measurements in figure 7(*a*i-*b*i) show that for short waves, the wave motion had only a negligible effect on the propagation of the gravity current fronts (x_- and x_+). In this case, orbital velocities decrease significantly down through the water column (see figure 3). Hence, near the bed the effect of the free surface was minimal. However, as the wave period increased, the wave motion had a more pronounced effect on the gravity current dynamics. It was observed, see figure 7(*b*i,*c*i), that wave action reduced the propagation of the upstream (x_+) gravity current and enhanced the propagation of the downstream (x_-) gravity current. The measured positions are compared to the theoretical model (4.7) with the wave component turned off. For the largest wave amplitudes the asymmetry in the gravity front position no longer appears to be linear. This can be seen from the differences in the total length graphs, figure 7(*a*ii,*b*ii,*c*ii), suggesting a more complex interaction than the outlined theoretical model.

The experimental measurements confirm that to leading order the total length of the gravity current is reasonably predicted by (4.8*a*). However, this statement is not valid for long waves, figure 7(*c*ii), where the total length of the current diverges from theory and appears to increase with wave height. The likely physical explanation is that the increased orbital motion near to the floor (found for long waves) generates a large shear turbulent boundary layer which enhances mixing at the front of the gravity current (see § 5.4).

5.3. *Centre of the gravity current*

The current centre, $\mathscr{X}$, was estimated by determining the midpoint position of the upstream x_+ and downstream x_- leading fronts. The movement of the gravity current

https://doi.org/10.1017/jfm.2013.112 Published online by Cambridge University Press

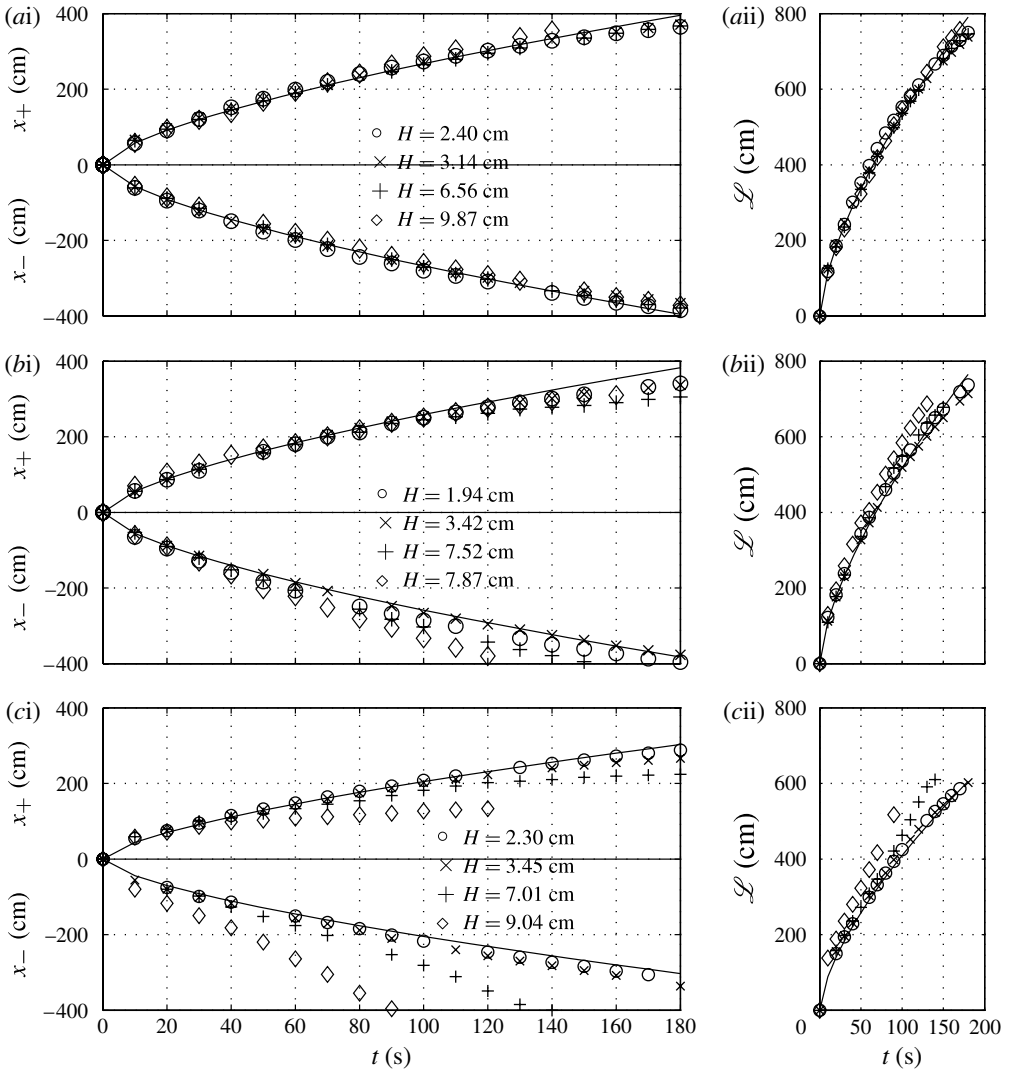


FIGURE 7. Comparison of the (i) upstream (x_+) and downstream (x_-) current fronts and (ii) total length ($\mathscr{L} = x_+ - x_-$) for gravity currents ($V_r = 1200\ \text{cm}^3$ and $g'_r = 40\ \text{cm s}^{-2}$) propagating in the presence of waves, $T =$ (*a*) 1.00 s, (*b*) 1.60 s, (*c*) 2.46 s, are shown as a function of time. The laboratory experiments (◯, ×, + and ◇) are compared with theory (4.7) with the wave component turned off (solid lines).

centre is plotted in figure 8 as a function of time for different wave forcing. A least-squares line was fitted to the data; the gradient provided an experimental advection of the gravity current centre. Owing to the potential experimental error generated by the release of the saline, the origin was not taken into account in determining these lines of best fit.

Figure 8(*a*) shows how the gravity current centre was affected by wave action for a fixed wave height and varying wave periods. For short wave periods, the Stokes drift near to the rigid floor is small and the mean Lagrangian velocity is positive as it is dominated by the mean flow generated by oscillatory boundary layers. The direction

https://doi.org/10.1017/jfm.2013.112 Published online by Cambridge University Press

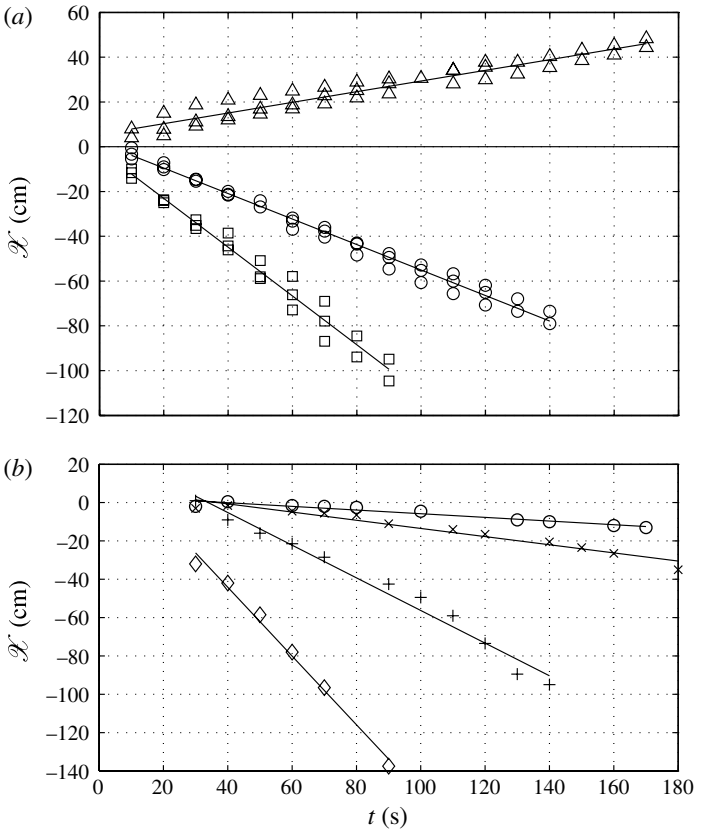


FIGURE 8. The position of the gravity current centre, $\mathscr{X}$, plotted as a function of time for different wave conditions. The solid lines are lines of best fit. In (*a*), $V_r = 1000$ cm^3, $g'_r = 50$ cm s^{-2}, $H = 6$ cm $\pm$ 0.5 cm, and T varied as: $\triangle$, 0.80 s; $\bigcirc$, 1.60 s; and $\square$, 2.46 s respectively (test cases W2, W4 and W6 in table 1). In (*b*), $V_r = 1200$ cm^3, $g'_r = 40$ cm s^{-2}, $T = 2.46$ s and H varied as: $\bigcirc$, 2.30 cm; $\times$, 3.45 cm; $+$, 7.01 cm; and $\Diamond$, 9.04 cm (test cases in figure 7*c*).

of mean advection changes sign as wave period increases. This is reflected in the observations in figure 8(*a*). For each test condition the experiment was repeated three times. Although there is some scatter in the results the direction and magnitude of the mean advection remains consistent.

Figure 8(*b*) shows the variation of the centre with time for fixed wave period and varying wave amplitude (corresponding to the results in figure 7*c*). Since the period, $T = 2.46$ s, is in the long-wave regime, the current is advected in the wave direction. In all cases, in figure 8(*b*), a negative advection was observed and the rate of advection increased significantly as the wave amplitude increased. This is in agreement with (4.8*b*) that predicts an amplitude-squared relation to the centroid position.

The results show that the centre of the gravity current was advected at a constant speed, which was dependent on the wave conditions. These observations are in agreement with (4.9), that states the speed of the gravity current centre is correlated with the mean Lagrangian velocity. As for the case of uniform ambient flows (Hallworth *et al.* 1998; Hogg *et al.* 2005), we correlated the mean ambient

https://doi.org/10.1017/jfm.2013.112 Published online by Cambridge University Press

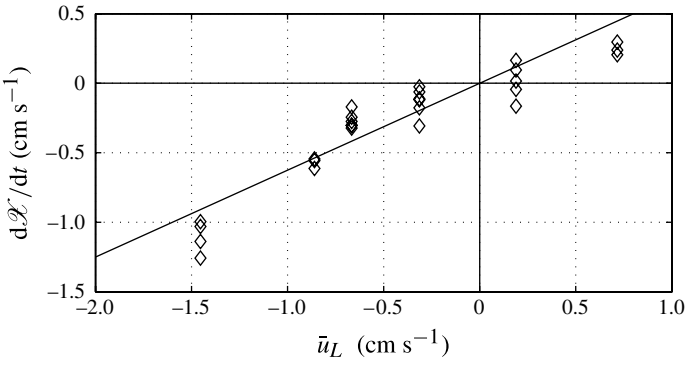


FIGURE 9. Variation of the bulk velocity of the gravity current centre, $d\mathscr{X}/dt$, with the Lagrangian velocity, $\bar{u}_L$, adjacent to the boundary averaged in a thin layer. The line of best fit through the origin is plotted with gradient 0.63 and correlation coefficient of 0.93.

flow ($\bar{u}_L$ defined by (3.10)) with the advection velocity of the gravity current in order to determine the empirical coefficient α given as

$$\frac{d\mathscr{X}}{dt} = \alpha \bar{u}_L. \tag{5.2}$$

For all tests a linear least-squares fit was applied to estimate $d\mathscr{X}/dt$ and $\bar{u}_L$ was taken from the LDV measurements (figure 4). The mean correlation coefficient for the linear fit was 0.96 with a standard deviation of 0.06. Typical results can be seen in figure 8. The scatter plot of the mean advection speed of the gravity current versus the averaged Lagrangian velocity in a layer adjacent to the floor is shown in figure 9. A line of best fit to the data was estimated, giving a coefficient $\alpha = 0.63$ with a correlation coefficient of 0.93. The gradient is comparable to the value of $\alpha = 0.6$ determined by Hallworth *et al.* (1998) and Hogg *et al.* (2005) for gravity currents propagating in uniform ambient flows, except the confidence limit here is lower.

5.4. *The structure of gravity current fronts*

The shape of the gravity current fronts moving upstream and downstream was analysed using the standard light attenuation method and an LIF system. The dye attenuation provides a cross-stream-integrated method of analysing the distribution of dye (as a proxy for salinity). The LIF method provides an instantaneous view of the distribution of dye within a narrow vertical plane. These contrasting methods of visualization provide different insight into how the shape and instabilities of the gravity current head develop. For practical reasons, the LIF images could only be captured at fixed positions for a small number of tests while the dye attenuation images were collected over the entire test section.

In the absence of waves, the width-averaged profiles of the upstream and downstream gravity current heads should be identical. However, owing to the turbulent instabilities along the gravity current interface, some small differences were observed between the upstream and downstream fronts, see figure 10.

In the presence of waves, figure 11, the two heads tend to display a much larger asymmetry, similar to that observed in studies of gravity currents in uniform flows (Hallworth *et al.* 1998). For short-period waves, both Stokes drift velocity and mean shear are weak, and as a consequence the asymmetry of the shape of the current

https://doi.org/10.1017/jfm.2013.112 Published online by Cambridge University Press

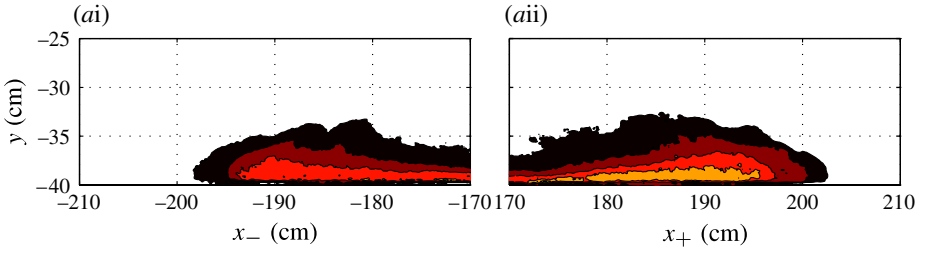


FIGURE 10. (Colour online) Dye concentration profile: density profiles of gravity currents ($V_r = 1000$ cm^3 and $g'_r = 50$ cm s^{-2}) in the absence of waves.

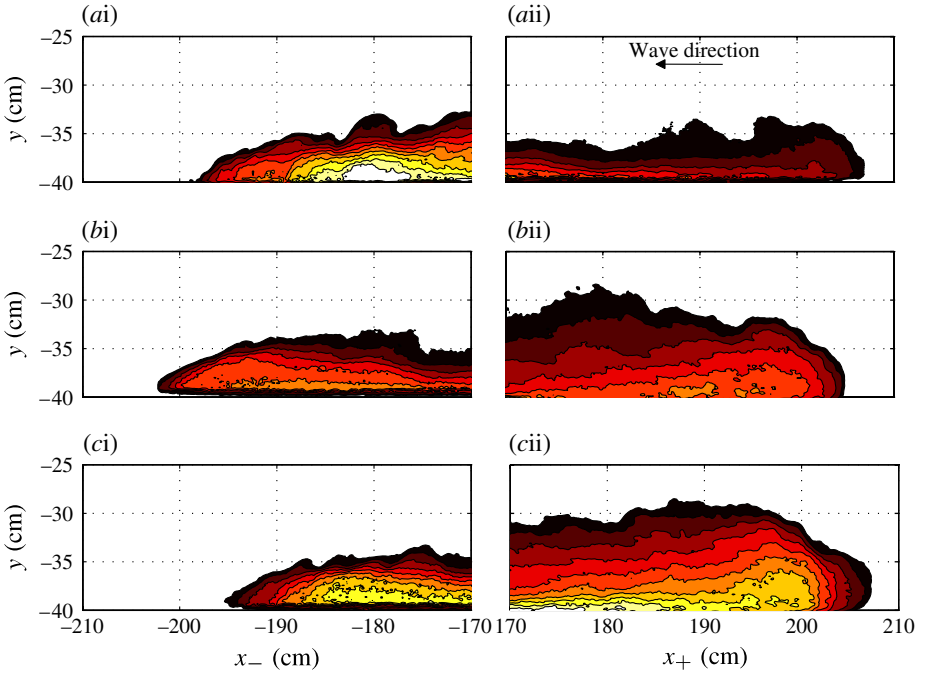


FIGURE 11. (Colour online) Dye concentration profile: density profiles of gravity currents ($V_r = 1000$ cm^3 and $g'_r = 55$–60 cm s^{-2}) in the presence of free-surface waves: T and $H =$ (*a*) 0.80 s, 6.49 cm; (*b*) 1.60 s, 6.05 cm and (*c*) 2.46 s, 7.00 cm respectively.

head remains small. However, for long waves the shape of the gravity current in the wave direction was observed to be much more angular and flatter than the equivalent gravity current propagating against the wave direction. Against the wave direction, the current was more rounded with a thicker mixing region between the gravity current and ambient water, see figure 11(*b*ii,*c*ii).

As expected, behind the head there were significant variations in the gravity current height. Xue, Xu & Droegemeier (1997) provide a physical explanation, which is interpreted in terms of the mean shear in the ambient flow. Since the upstream moving head contains positively signed baroclinic vorticity it combines with the negative vorticity in the ambient flow to raise the head of the current – a process which Xue

https://doi.org/10.1017/jfm.2013.112 Published online by Cambridge University Press

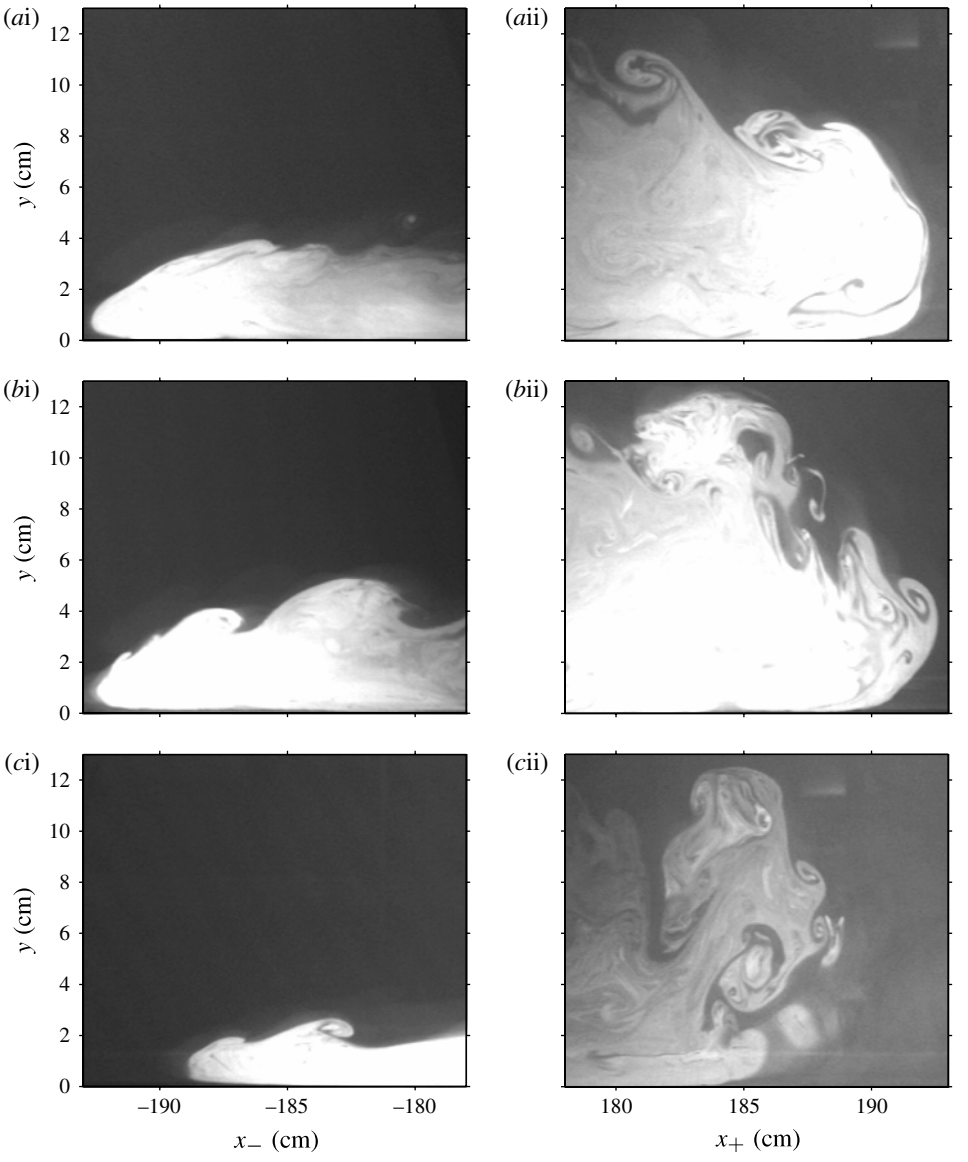


FIGURE 12. LIF images of gravity currents ($V_r = 1000\,\mathrm{cm}^3$ and $g'_r = 55$–$60\,\mathrm{cm\,s}^{-2}$) propagating with (i) and against (ii) the wave direction. The wave period, T, and wave height, H, are given as: 0.80 s, 6.49 cm; (*b*) 1.60 s, 6.05 cm and (*c*) 2.46 s, 7.00 cm respectively.

et al. term vorticity ventilation. The opposite process occurs in the head moving in the wave direction. Simpson & Britter (1979) studied the effect of shearing rather than a uniform incident flow; their results appear to support the conclusion of Xue *et al.* (1997).

Hacker *et al.* (1996) observed that Kelvin–Helmholtz-like waves forming along the density interface do not preserve their structure across the width of the flume and so cannot be identified by the width-average measurements. This observation was confirmed by comparing the results from the width-averaged profiles (figure 11) and

https://doi.org/10.1017/jfm.2013.112 Published online by Cambridge University Press

the thin-slice images from LIF (figure 12). The use of a laser to generate a thin light sheet provides a method of visualizing a thin vertical planar image of the structure of the gravity current and the shape of the instabilities along the density interface, see figure 12. The LIF images show the two heads of the current at fixed positions upstream and downstream in the presence of waves. These images provide a snapshot of the mixing within the head and broadly support the width-averaged optical results. In addition LIF provides further evidence of the complex interaction between the gravity current and wave fields for highly oscillatory flows, as shown in figure 12(*c*). Further analysis is required to provide a physical explanation of these results.

6. Concluding remarks

We have described a study of the effect of free-surface progressive waves on the movement of inertially dominated dense saline gravity currents. It has been demonstrated that the gravity current head moves backwards and forwards at the frequency and amplitude of the oscillatory wave-induced flow motion near the floor. The combination of viscous streaming motion and Stokes drift generates a mean mass flux profile beneath the free surface that advects the gravity current centre at a speed correlated with the depth-averaged Lagrangian mean velocity adjacent to the bed. For short waves, Stokes drift velocity near to the floor is negligible and the gravity current is advected in the opposite direction to the wave direction. But for long waves, the current is advected in the wave direction because Stokes drift dominates transport near to the floor.

The behaviour of saline gravity currents in a wave field is similar, in some respects, to currents generated by an instantaneous release moving in an ambient flow (Hallworth *et al.* 1998; Hogg *et al.* 2005; Slim & Huppert 2008). Indeed our modelling approach draws from this body of work, although there are some differences as highlighted in the combined effect of Stokes drift and the Eulerian-averaged flow. As with Hallworth *et al.* (1998), the centre of the current is advected at a fraction of the mean ambient flow – here we observe a slightly larger correlation of 0.63 to a mean Lagrangian velocity at the bed. This relationship was found for a broad range of inertia-dominant gravity currents ($600\ \mathrm{cm}^3 < V_r < 1800\ \mathrm{cm}^3$ and $20\ \mathrm{cm\ s}^{-2} < g'_r < 50\ \mathrm{cm\ s}^{-2}$) in the presence of shallow water waves ($0.8\ \mathrm{s} < T < 2.5\ \mathrm{s}$ and $2.0\ \mathrm{cm} < H < 8.0\ \mathrm{cm}$). Although asymmetry in the downstream and upstream gravity current heads was observed the correlation of the profiles with the ambient shearing flow, governed by the wave condition and profile, remains quite complex. It is clear that the direction of the gravity current, relative to the wave direction, is important in determining the characteristics of a gravity current and the related mixing and dispersion. Although some general description could be given with regard to the different wave regimes, quantifying this in terms of the expected concentration remains to be done.

There are a number of natural extensions to this work that are worth considering, such as the release of fresh water or warmer industrial fluid. Practical applications occur in estuarine flows and in coastal regions where waves may be the dominant characteristic. For short waves, the Stokes drift component is largest at the free surface and decreases exponentially with depth; in contrast Stokes drift for long waves is only weakly dependent on depth. This suggests that the direction in which buoyant gravity currents are advected by the wave-induced mass flux near the free surface, may be opposite to that experienced by dense gravity currents.

https://doi.org/10.1017/jfm.2013.112 Published online by Cambridge University Press

Acknowledgements

T.O.R. was supported by EPSRC during his PhD. The authors express their thanks and gratitude to L. Ansdell and K. Harvey for their technical support.

REFERENCES

ADDUCE, C., SCIORTINO, G. & PROIETTI, S. 2012 Gravity currents produced by lock exchanges: experiments and simulations with a two-layer shallow-water model with entrainment. *J. Hydraul. Engng* **138** (2), 111–121.

BAGNOLD, R. A. 1946 Sand movements by waves: some small-scale experiments with sand of very low density. *J. Inst. Civil Engrs* **27**, 447–469.

BENJAMIN, T. B. 1968 Gravity currents and related phenomena. *J. Fluid Mech.* **31**, 209–248.

BÜHLER, J., WRIGHT, S. J. & KIM, Y. 1991 Gravity currents advancing into a coflowing fluid. *J. Hydraul. Res.* **29** (2), 243–257.

CHAMBERLAIN, N. 2000 Wave-induced mixing within a gravity-driven surface current. PhD thesis, Department of Civil and Environmental Engineering, Imperial College of Science, Technology and Medicine.

DAHM, W. J. A. & DIMOTAKIS, P. E. 1990 Mixing at large Schmidt number in the self-similar far field of turbulent jets. *J. Fluid Mech.* **217**, 299–330.

DYKE, P. P. G & BARSTOW, S. F. 1981 Wave induced mass transport: theory and experiment. *J. Hydraul. Res.* **19**, 89–105.

EAMES, I. 2008 Settling of particles beneath water waves. *J. Phys. Oceanogr.* **38**, 2846–2853.

EAMES, I. & MCINTYRE, M. 1999 On the connection between Stokes drift and Darwin drift. *Math. Proc. Camb. Phil. Soc.* **126**, 171–174.

FOURIER, J. 1890 *Mémoire sur la propagation de la chaleur dans les corps solides, présenté le 21 décembre 1807 à l'Institut national – Nouveau Bulletin des sciences par la Société philomatique de Paris* I (6). Paris: Bernard. March 1808. pp. 112–116. Reprinted in 'Mémoire sur la propagation de la chaleur dans les corps solides'. *Joseph Fourier – Œuvres complètes, tome 2.* pp. 215–221.

HACKER, J., LINDEN, P. F. & DALZIEL, S. B. 1996 Mixing in lock-release gravity currents. *Dyn. Atmos. Oceans* **24**, 183–195.

HALLWORTH, M. A., HOGG, A. J & HUPPERT, H. E. 1998 Effects of external flow on compositional and particle gravity currents. *J. Fluid Mech.* **359**, 109–142.

HOGG, A. J. & HUPPERT, H. E. 2001 Spreading and deposition of particulate matter in uniform flows. *J. Hydraul. Res.* **39**, 1–14.

HOGG, A. J., HUPPERT, H. E. & HALLWORTH, M. A. 2005 On gravity currents driven by constant fluxes of saline and particle-laden fluid in the presence of a uniform flow. *J. Fluid Mech.* **539**, 349–385.

HUPPERT, H. E. 2006 Gravity currents: a personal perspective. *J. Fluid Mech.* **554**, 299–322.

HUPPERT, H. E. & SIMPSON, J. E. 1980 Slumping of gravity currents. *J. Fluid Mech.* **99**, 785–799.

JOHNS, B. 1970 On the mass transport induced by oscillatory flow in a turbulent boundary layer. *J. Fluid Mech.* **43**, 177–185.

VON KÁRMÁN, T. 1940 The engineer grapples with nonlinear problems. *Bull. Am. Math. Soc.* **46**, 615–683.

KRANENBURG, C. 1993 Gravity-current fronts advancing into horizontal ambient flow. *J. Hydraul. Engng* **119**, 369–379.

LIGHTHILL, J. 1978 *Waves in Fluids*, 1st edn. Cambridge University Press.

LONGUET-HIGGINS, M. S. 1953 Mass transport in water waves. *Phil. Trans. R. Soc. Lond.* A **245**, 535–581.

LOWE, R. J., ROTTMAN, J. W. & LINDEN, P. F. 2005 The non-Boussinesq lock-exchange problem. Part 1. Theory and experiments. *J. Fluid Mech.* **537**, 101–124.

MARINO, B. M., THOMAS, L. P. & LINDEN, P. F. 2005 The front condition for gravity currents. *J. Fluid Mech.* **536**, 49–78.

https://doi.org/10.1017/jfm.2013.112 Published online by Cambridge University Press

MILNE-THOMSON, L. M. 1968 *Theoretical Hydrodynamics*, 6th edn. Macmillan.

MONISMITH, S. G., COWEN, E. A., NEPF, H. M., MAGNAUDET, J. & THAIS, L. 2007 Laboratory observations of mean flows under surface gravity waves. *J. Fluid Mech.* **573**, 131–147.

MUESCHKE, N. J., SCHILLING, O., YOUNGS, D. L. & ANDREWS, M. J. 2009 Mixing at large Schmidt number in the self-similar far field of turbulent jets. *J. Fluid Mech.* **632**, 17–48.

NG, C.-O. & FU, S.-C. 2002 On the propagation of a two-dimensional viscous density current under surface waves. *Phys. Fluids* **14** (3), 970–984.

NIELSEN, P. 1992 *Coastal Bottom Boundary Layers and Sediment Transport*. World Scientific.

ROBINSON, T. O. 2007 Gravity current in the presence of water waves. PhD thesis, University College London.

ROTTMAN, J. W. & SIMPSON, J. E. 1983 Gravity currents produced by insantaneous releases of a heavy fluid in a rectangular channel. *J. Fluid Mech.* **135**, 95–110.

RUSSELL, R. C. H. & OSORIO, J. D. C. 1957 An experimental investigation of drift profiles in a closed channel. *Coast. Engng* **1**, 171–183.

SHIN, J. O., DALZIEL, S. B. & LINDEN, P. F. 2004 Gravity currents produced by lock exchange. *J. Fluid Mech.* **521**, 1–34.

SIMPSON, J. E. 1997 *Gravity Currents in the Environment and the Laboratory*, 2nd edn. Cambridge University Press.

SIMPSON, J. E. & BRITTER, R. E. 1979 The dynamics of the head of a gravity current advancing over a horizontal surface. *J. Fluid Mech.* **94**, 477–495.

SKOGNESS, K. & JOHANSEN, Ø. 2004 Statmap – a three-dimensional model for oil spill risk assessment. *Environ. Model. Softw.* **19**, 727–736.

SLIM, A. C. & HUPPERT, H. E. 2008 Gravity currents from a line source in an ambient flow. *J. Fluid Mech.* **606**, 1–26.

STOKES, G. G. 1847 On the theory of oscillatory waves. *Trans. Camb. Phil. Soc.* **8**, 441–455.

SWAN, C. 1990 Convection within an experimental wave flume. *J. Hydraulic. Res.* **28**, 273–282.

SWAN, C. & SLEATH, J. F. A. 1990 A second approximation to the time-mean Lagrangian drift beneath a series of progressive gravity waves. *Ocean Engng* **17**, 65–79.

WRIGHT, L. D., FRIEDRICHS, C. T. & SCULLY, M. E. 2001 Effects of ambient currents and waves on gravity-driven sediment transport on continental shelves. *Mar. Geol.* **175**, 25–45.

WRIGHT, L., WISEMAN, W., BORNHOLD, D., PRIOR, D., SUHAYDA, J., KELLER, G., YANG, Z.-S. & FAN, Y. 1988 Marine dispersal and deposition of yellow river silts by gravity-driven underflows. *Nature* **332**, 629–632.

XU, Z. & BOWEN, A. J. 1994 Wave- and wind-driven flow in water of finite depth. *J. Phys. Oceanogr.* **24**, 1850–1866.

XUE, M., XU, Q. & DROEGEMEIER, K. K. 1997 A theoretical and numerical study of density currents in non-constant shear flows. *J. Atmos. Sci.* **54**, 1998–2019.

https://doi.org/10.1017/jfm.2013.112 Published online by Cambridge University Press